PHYSICAL REVIEW D **88,** 055017 (2013)

Simultaneous enhancement in $\gamma\gamma$, $b\bar{b}$ and $\tau^+\tau^-$ rates in the NMSSM with nearly degenerate scalar and pseudoscalar Higgs bosons

Shoaib Munir,* Leszek Roszkowski,†,‡ and Sebastian Trojanowski§

National Centre for Nuclear Research, Hoża 69, 00-681 Warsaw, Poland

(Received 16 May 2013; published 23 September 2013)

We propose an experimental test of a scenario in the next-to-minimal supersymmetric standard model in which both the lightest scalar and the lightest pseudoscalar Higgs bosons have masses around 125 GeV. The pseudoscalar can contribute significantly to the $\gamma\gamma$ rate at the LHC due to light Higgsino-like charginos in its effective one-loop coupling to two photons. Such charginos are obtained for small values of the μ_{eff} parameter, which also results in enhanced $b\bar{b}$ and $\tau^+\tau^-$ rates compared to those expected for a standard model (SM) Higgs boson. This scenario should result in a clear discrepancy between the observed rates in these three decay channels and those in the WW and ZZ channels, since the pseudoscalar does not couple to the W and Z bosons. However, in the dominant gluon fusion production mode, the pseudoscalar will stay hidden behind the SM-like scalar Higgs boson, and in order for it to be observable, the associated $b\bar{b}h$ production mode has to be considered, the cross section for which is tiny in the SM but $\tan\beta$-enhanced in supersymmetry. We analyze the constrained next-to-minimal supersymmetric standard model with nonuniversal Higgs sector parameters and identify regions of its parameter space where the lightest pseudoscalar with mass around 125 GeV and strongly enhanced $\gamma\gamma$ (up to 60%), $b\bar{b}$ and $\tau^+\tau^-$ rates in the $b\bar{b}h$ mode can be obtained.

DOI: 10.1103/PhysRevD.88.055017 PACS numbers: 12.60.Jv, 12.60.−i, 14.80.Ec

I. INTRODUCTION

Since its discovery at the LHC in July 2012 [1,2], the CMS and ATLAS collaborations have accumulated more data and updated their results on the Higgs boson. In the early results, a considerable enhancement in the $\gamma\gamma$ and ZZ rates compared to the standard model (SM) prediction was noted near ~125 GeV at the ATLAS detector. According to the CMS data, the signal strength, $\sigma/\sigma_{\mathrm{SM}}$, was consistent with the SM prediction in the ZZ channel, but an enhancement in the $\gamma\gamma$ channel was observed there as well. However, the figures from both experiments have changed in the latest results released after the collection of ~20/fb of data [3,4]. The signal strengths measured by the CMS have now fallen down to SM-like values, 0.78 ± 0.27 and $0.91^{+0.30}_{-0.24}$ in the $\gamma\gamma$ and ZZ decay channels, respectively, with the mean value of the boson mass being 125.6 ± 0.64 GeV.

The ATLAS Collaboration, on the other hand, still reports sizable excesses, $\sigma/\sigma_{\mathrm{SM}} = 1.65 \pm 0.35$ in the $\gamma\gamma$ channel with the mass measurement yielding 126.8 ± 0.73 GeV, and $\sigma/\sigma_{\mathrm{SM}} = 1.7 \pm 0.5$ in the ZZ channel with mass at $124.3^{+0.55}_{-0.4}$ GeV. Moreover, broad peaks consistent with a 125 GeV boson have now also been observed in the $H \to WW \to 2l2\nu$ channel in the two detectors. Importantly, the best-fit signal strength in this channel is SM-like according to both CMS and ATLAS, with a measured value of 0.76 ± 0.21 at the former and of 1.01 ± 0.31 at the latter. In the $b\bar{b}$ decay channel, although no significant excess has been observed above the SM background at either CMS or ATLAS, fitted signal strength values at $m_h = 125$ GeV have been obtained by the two collaborations for some individual Higgs boson production modes. The best-fit values provided by the CMS collaboration read 0.7 ± 1.4 for vector boson fusion (VBF), $1.0^{+0.5}_{-0.5}$ for Higgs-strahlung off a vector boson (Wh/Zh) and $0.74^{+1.34}_{-1.30}$ for associated production off top quarks ($t\bar{t}h$). The ATLAS Collaboration has recently provided a fitted value of 0.2 ± 0.64 for the Wh/Zh production mode only. In the $\tau^+\tau^-$ channel, an excess of events over a broad m_h range was reported by the CMS Collaboration with a best-fit $\sigma/\sigma_{\mathrm{SM}} = 1.1 \pm 0.4$ at 125 GeV. At ATLAS, however, no excess has so far been observed in this channel also, and a fitted value at $m_h = 125$ GeV, which is SM-like but with a very large error, can be noted in Ref. [5]. We should point out here that neither of the two collaborations has provided any measurements of the signal strength in the $b\bar{b}$ and $\tau^+\tau^-$ decay channels for associated Higgs boson production off bottom quarks ($b\bar{b}h$).

Since the first announcements of the discovery of the boson, there have been many attempts to interpret the observed data in light of various supersymmetric (SUSY) extensions of the SM [6–15]. In the context of the minimal supersymmetric standard model (MSSM), the observed signal can be interpreted as being due to the lightest Higgs boson of the model, h. In the MSSM constrained at the grand unification theory (GUT) scale, referred to as the CMSSM [16], h can attain a mass around the measured central value only if the SUSY-breaking scale, M_{SUSY}, is

*Shoaib.Munir@fuw.edu.pl
†On leave from the University of Sheffield, Sheffield, UK.
‡L.Roszkowski@sheffield.ac.uk
§Sebastian.Trojanowski@fuw.edu.pl

close to or larger than 1 TeV, while also satisfying other important phenomenological constraints. In the next-to-minimal supersymmetric standard model (NMSSM) [17,18] (see, e.g., Refs. [19,20] for recent reviews), it has been shown that either of the two lightest CP-even Higgs bosons, h_1 and h_2, can easily be SM-like with mass around 125 GeV [21,22]. In fact in this model it is possible to have h_1 and h_2 almost degenerate in mass around 125 GeV [10], so that the observed signal is actually a superposition of two individual peaks due to each of these, which cannot be independently resolved.

In the GUT-constrained version of the NMSSM (CNMSSM) [18,23–25], in analogy with the CMSSM, it has been found that in order to obtain h_1 as heavy as 125 GeV, $M_{\rm SUSY}$ at or above 1 TeV is needed even with relevant phenomenological constraints imposed [14]. Alternatively, a SM-like h_2 with mass $\sim$125 GeV is easily achievable [14]. Relaxing slightly the universality conditions by disunifying the masses of the scalar Higgs doublets m_{H_u} and m_{H_d} from the scalar mass parameter m_0 and the soft Higgs trilinear coupling parameters A_λ and A_κ from the unified soft Yukawa coupling A_0 makes it relatively easy to obtain SM-like h_1 or h_2 around 125 GeV [26]. Here we refer to such a model with nonuniversal Higgs sector parameters as CNMSSM-NUHM. The scenario with mass degenerate h_1 and h_2 satisfying also other phenomenological constraints has also been pursued with much interest in the CNMSSM-NUHM [10,12].

Even though the latest results from CMS seem to favor a SM-like Higgs boson, those from ATLAS do so only partially, and it is still possible for the observed boson to be a nonstandard one. The inconsistencies between the various measurements and fluctuations in the data leave ample room for speculation in this regard. Therefore, in this article, we propose an experimental test of a scenario, not investigated hitherto, in which the lightest pseudoscalar, a_1, of the NMSSM is almost degenerate in mass with the lightest $\sim$125 GeV scalar, h_1. Such an a_1 can have a sizeable one-loop effective coupling to $\gamma\gamma$ in the presence of a light Higgsino-like chargino in the loop. Thus, with decreasing mass of such a chargino, one should expect a rise in the signal rate defined, for a general Higgs boson h_i, as

$$R_X^Y(h_i) = \frac{\sigma(Y \to h_i)}{\sigma(Y \to h_{\rm SM})} \times \frac{{\rm BR}(h_i \to X)}{{\rm BR}(h_{\rm SM} \to X)}, \qquad (1)$$

where $h_{\rm SM}$ is a SM Higgs boson with the same mass as h_i and X denotes any one of its allowed SM decay channels. Y stands for the various possible Higgs boson production modes at the LHC, which include gluon fusion (ggh), VBF, Wh/Zh[1] and $t\bar{t}h/b\bar{b}h$. However, for $X = \gamma\gamma$, despite the non-negligible size of the second term in the product on the right-hand side of Eq. (1), no net enhancement in the $\gamma\gamma$ rate of a_1 with decreasing chargino mass would be visible in the ggh production mode. The reason is that the first term in the product always has a very small magnitude due to a highly reduced effective coupling of a_1 to two gluons compared to that of a SM Higgs boson, which is dominated by the top quark loop, thus nullifying the overall effect.

The overall enhancement in $R_X^Y(a_1)$ due to a light chargino should instead be visible in the $b\bar{b}h$ production mode since, as we shall see, the conditions necessary to obtain a light chargino also result in an enhanced coupling of a_1 to $b\bar{b}/\tau^+\tau^-$. In fact, one should thus obtain a simultaneous enhancement in the signal rates of the three channels, $\gamma\gamma$, $b\bar{b}$ and $\tau^+\tau^-$ (collectively referred to as X henceforth). We point out here that, while the enhancement in the $b\bar{b}$ and $\tau^+\tau^-$ channels only is in principle possible even with a light MSSM-like scalar Higgs boson for large $\tan\beta$, the above "triple enhancement" should be a clear signature of our proposed scenario. For this reason we shall investigate $b\bar{b}h$ Higgs production mode here, emphasizing the importance of a measurement of the signal rate in this mode, which is very subdominant for a SM Higgs boson and is therefore generally considered to be of less interest. In contrast, in SUSY it is enhanced by $\tan^2\beta$ [27] and can therefore be potentially very interesting.

In the $b\bar{b}h$ channel, the a_1 could be partially responsible for a net enhancement in the signal rate, $R_X^{bb}({\rm obs})$, in the X decay channels measured at the LHC. However, being a pseudoscalar, it would not contribute to the WW and ZZ channels (denoted collectively by V), so that, assuming h_1 to be exactly SM-like,

$$R_X^{bb}({\rm obs}) \equiv \frac{\sigma_X^{bb}({\rm obs})}{\sigma_X^{bb}(h_{\rm SM})} = R_X^{bb}(h_1) + R_X^{bb}(a_1) \simeq 1 + R_X^{bb}(a_1)$$
$$\text{and} \quad R_V^{bb}({\rm obs}) = R_V^{bb}(h_1) \simeq 1. \qquad (2)$$

Furthermore, a difference in the mass measurements in the X and V modes would also provide a hint for mass degenerate h_1 and a_1. Such a degeneracy would imply that the signal observed in the X channels should in fact be interpreted as the "sum" of two individual peaks due to h_1 and a_1, while the peaks in the V modes correspond to h_1 alone. h_1 is still SM-like in this scenario due to a significant singlet component even though $\tan\beta$ can take fairly large values [28]. Since this scenario is compatible with a SM-like scalar Higgs boson, it is also not in conflict with the recent CMS measurements in the ZZ mode which disfavor the pure pseudoscalar hypothesis [29,30].

We identify regions of the CNMSSM-NUHM parameter space where both h_1 and a_1 with masses around 125 GeV can be obtained, expecting that a discrepancy between X and V rates will be seen by CMS and ATLAS collaborations in a focused analysis of the $b\bar{b}h$ production mode. We further confine ourselves only to the regions where the above-mentioned triple enhancement can be obtained, serving as a clear signature of this scenario. We investigate the impact of other important experimental constraints on these

[1]We note here that the VBF and Wh/Zh production modes are irrelevant for a pseudoscalar Higgs boson.

regions. These include the limits from direct SUSY searches released by ATLAS with $\sim$20/fb of data as well as from the dark matter (DM) relic density measurements. We also require the corresponding parameter space to satisfy the recently announced positive $\mathrm{BR}(B_s \to \mu^+\mu^-)$ measurement by the LHCb Collaboration.

The article is organized as follows. In Sec. II we discuss the possibility of observing an enhancement in the $\gamma\gamma$ and $b\bar{b}/\tau^+\tau^-$ rates at the LHC due to a $\sim$125 GeV pseudoscalar Higgs boson. In Sec. III we define the model's parameter space. In Sec. IV we describe the experimental constraints applied in our scans, present our numerical results and discuss their salient features. We summarize our findings in Sec. V.

II. ENHANCEMENT IN THE OBSERVED $\gamma\gamma$ RATE DUE TO A LIGHT PSEUDOSCALAR

In this section we present some analytical details of the mentioned NMSSM scenario in which the correlation between the $\gamma\gamma$ and WW/ZZ rates can be altered. One way to achieve this is with mass degenerate lightest doubletlike scalar Higgs, h_1, and lightest singletlike pseudoscalar, a_1.

A. Pseudoscalar mass

We first discuss the conditions that are necessary to obtain a $\sim$125 singletlike a_1, which couples to two photons through loops of fermions and charginos only. Starting from the 2×2 pseudoscalar mass matrix (after rotating away the Goldstone mode) [19], one can obtain the approximate expression,

$$m_{a_1}^2 \simeq -3\kappa s A_\kappa^{\mathrm{SUSY}} - \frac{M_{P,12}^4}{M_{P,11}^2}. \quad (3)$$

In the above equation, $M_{P,12}^2 \simeq \lambda(A_\lambda^{\mathrm{SUSY}} - 2\kappa s)v$ is the off-diagonal entry of the pseudoscalar mass matrix, where $v \equiv \sqrt{v_u^2 + v_d^2} \simeq 174$ GeV, with v_u and v_d being the vacuum expectation values (vevs) of the u-type and d-type Higgs doublets, respectively, and $A_{\lambda/\kappa}^{\mathrm{SUSY}}$ denoting $A_{\lambda/\kappa}$ at M_{SUSY}. $M_{P,11}^2 \simeq \mu_{\mathrm{eff}} B_{\mathrm{eff}} \tan\beta$, with $\mu_{\mathrm{eff}} \equiv \lambda s$ (s being the vev of the singlet field S), $B_{\mathrm{eff}} \equiv A_\lambda^{\mathrm{SUSY}} + \kappa s$ and $\tan\beta \equiv v_u/v_d$, is the diagonal term corresponding to the mass squared of the doubletlike heavy pseudoscalar, a_2. The leading term in Eq. (3) implies that, for positive κ, which we will assume here, the condition of the positivity of $m_{a_1}^2$ depends predominantly on the relative signs of μ_{eff} and A_κ at M_{SUSY}. This condition thus has some important repercussions when A_κ and A_λ are taken as input parameters at the GUT scale. Assuming the leading term to be positive so that the correct m_{a_1} is achieved by adjusting the free parameters in it, the negative contribution from the second term should be kept close to zero. This would require $M_{P,11}^2 \gtrsim M_{P,12}^4$. We explain how this can be achieved for negative and positive μ_{eff} in the following.

For $\mu_{\mathrm{eff}} < 0$ (and therefore negative s, assuming positive λ), the first term in Eq. (3) is positive if $A_\kappa > 0$ at M_{SUSY}. In the second term, $M_{P,12}^4$ is positive definite, and $M_{P,11}^2$ must be positive for a nontachyonic a_2, which requires $B_{\mathrm{eff}} < 0$. For given $\tan\beta$ and μ_{eff}, $M_{P,11}^2$ is driven by the magnitude of B_{eff}, in order to enhance which A_λ should take smaller values (note that A_λ is bounded from above by $\kappa|s|$). However, A_λ at M_{SUSY} runs upward from its GUT value with falling negative A_0 owing to the contribution from the relevant term in its renormalization group equation (RGE) [19]. Hence, increasing negative A_0 diminishes the difference between the two terms in B_{eff}, reducing its size and in turn driving $M_{P,11}^2$ closer to zero. At the same time, $M_{P,12}$, which is a sum of $2\kappa|s|$ and A_λ, grows as A_λ increases, as opposed to $M_{P,11}^2$. Consequently, the ratio $\frac{M_{P,12}^4}{M_{P,11}^2}$ in Eq. (3) grows with decreasing A_0 and, for large negative values of the latter, can result in negative $m_{a_1}^2$. Note also that the running of A_κ in turn depends dominantly on A_λ. A_κ runs upward with A_λ as long as the latter is negative. When A_λ turns positive, A_κ runs in the opposite direction, owing to its RGE. Thus, A_κ in the leading term in Eq. (3) will have somewhat constrained GUT scale values that can yield correct m_{a_1}. On the other hand, for $\mu_{\mathrm{eff}} > 0$, the two terms in B_{eff} are both positive, and the cancellation described above does not occur.

In summary, the net effect of the interplay between various Higgs sector parameters is that for negative μ_{eff}, the values of A_0 at the GUT scale are bounded from below by the condition of the physicality of a_1. This constraint on A_0 causes a slight tension between m_{h_1} and m_{a_1}, since it is well known that in order to obtain h_1 which is SM-like with mass $\sim$125 GeV large negative values of A_0 are required for $M_{\mathrm{SUSY}} \sim 1$ TeV. For positive μ_{eff}, there is no such tension because A_0 is relatively free to take values that give large negative A_t at M_{SUSY}, as long as the correct a_1 mass can be achieved by adjusting other free parameters.

B. $\gamma\gamma$ decay of the pseudoscalar

Besides a singletlike a_1 with mass similar to that of the experimentally observed boson, this scenario also requires a low mass, $m_{\chi_1^\pm}$, of the lightest chargino. The effective coupling of a pseudoscalar a_i, with $i = 1, 2$, to two photons (see, e.g., Refs. [31,32]) is dominated by a light chargino in the loops and can be approximated by

$$C_{a_i}^{\mathrm{eff}}(\gamma\gamma) \simeq \frac{g_{a_1\chi_1^\pm\chi_1^\pm}}{\sqrt{\sqrt{2}G_F}\, m_{\chi_1^\pm}} A_{1/2}^{a_i}(\tau_i), \quad (4)$$

where $\tau_i = \frac{m_{a_i}^2}{4m_{\chi_1^\pm}^2}$. For $\tau_i \leq 1$, which is applicable here, with $m_{a_i} \simeq 126$ GeV and the light chargino obeying the lower limit, $m_{\chi_1^\pm} > 94$ GeV [33], the form factor $A_{1/2}^{a_i}(\tau_i) = \frac{1}{\tau_i}\arcsin^2\sqrt{\tau_i}$ [34] in the above equation lies in the range

$$1 < A_{1/2}^{a_i}(\tau_i) \lesssim 1.2. \tag{5}$$

The coupling of a_i to charginos in Eq. (4) can be written, following the notation of Ref. [19], as

$$g_{a_i\chi_1^\pm\chi_1^\pm} = i\left[\frac{\lambda}{\sqrt{2}}P_{i3}\sin\theta_U\sin\theta_V - \frac{g_2}{\sqrt{2}}(P_{i2}\cos\theta_U\sin\theta_V + P_{i1}\sin\theta_U\cos\theta_V)\right], \tag{6}$$

where θ_U, θ_V are the mixing angles for rotating the chargino interaction states to mass eigenstates, and P_{ij} are the entries of the mixing matrix that diagonalizes the pseudoscalar mass matrix. When the pseudoscalar weak eigenstates A_i^{weak} are expressed in the basis (H_{dI}, H_{uI}, S_I) [19], P_{i1} corresponds to H_{dI}, P_{i2} to H_{uI} and P_{i3} to S_I, respectively.

The first term in Eq. (6) implies that $\sin\theta_{U,V} \simeq 1$ (yielding a Higgsino-like $\chi_1^\pm$), $P_{13} \simeq 1$ and that larger values of λ are needed in order to enhance $C_{a_1}^{\mathrm{eff}}(\gamma\gamma)$ for the singletlike a_1. On the other hand, for the doubletlike pseudoscalar, a_2, an enhancement in $C_{a_2}^{\mathrm{eff}}(\gamma\gamma)$ requires either $\cos\theta_U\sin\theta_V$ or $\sin\theta_U\cos\theta_V$ to be non-negligible. This can be realized only in a very limited region of the parameter space where $M_2 \simeq \mu_{\mathrm{eff}}$ and not too large in order to keep $m_{\chi_1^\pm}$ low. Moreover, in this case, the mixing angles in the chargino sector read

$$\theta_{U,V} \simeq \arctan\left[\frac{\pm 2M_W^2\frac{1-\tan^2\beta}{1+\tan^2\beta} - 2\sqrt{(M_W^2+\mu_{\mathrm{eff}}^2)^2 - \mu_{\mathrm{eff}}^4}}{\sqrt{2}M_W\mu_{\mathrm{eff}}(1+\tan\beta)}\right], \tag{7}$$

where m_W is the mass of W boson. The sign of the first term implies that the enhancement can only be seen when a_2 has a leading H_{dI} component so that the term in Eq. (7) proportional to $\sin\theta_U\cos\theta_V$ is dominant. Evidently, in this case the $a_2 b\bar{b}$ coupling, and in turn $\mathrm{BR}(a_2 \to b\bar{b})$, will also get enhanced. Consequently, a contribution from a_2 will provide no significant excess in the $\gamma\gamma$ signal rate, defined in Eq. (1).

The above explanation also precludes such a scenario in the MSSM, where the pseudoscalar, A, is doubletlike. Besides, as noted in Ref. [35,36], in the MSSM in order to obtain the lightest CP-even Higgs boson, h, with mass around 125 GeV, m_A is required to be $\gtrsim 300$ GeV, which is the so-called decoupling regime of the model. On the other hand, while it is also possible to have a ~125 GeV H, the heavier CP-even Higgs boson of the MSSM, this can only be achieved for 95 GeV $< m_A <$ 110 GeV, in a tiny portion of the "nondecoupling regime." This region is, moreover, disfavored by the constraints from flavor physics [37,38].

In the fully constrained version of the NMSSM, unification of A_κ and A_0 at the GUT scale introduces tension between the masses of h_1 and a_1, not allowing both to acquire values $\lesssim 125$ GeV simultaneously. There, in order to obtain the correct h_1 mass, large negative values of A_0 are necessary so that the mixing term ($\frac{X_t}{M_{\mathrm{SUSY}}} \simeq \frac{A_t}{M_{\mathrm{SUSY}}}$) can be maximized. A light a_1, on the other hand requires small A_κ at M_{SUSY}, which in turn implies small A_κ at the GUT scale, owing to the effects of running. Moreover, small values of μ_{eff}, necessary to obtain light Higgsino-like charginos, additionally limit the running of A_t in the CNMSSM [14]. Therefore, to obtain a SM-like ~125 GeV h_1 and a pseudoscalar with a similar mass and a non-negligible $\gamma\gamma$ rate, one has to look beyond the MSSM and the CNMSSM; hence, we analyze the CNMSSM-NUHM here.

Through the mechanism explained above, a more precise measurement of the reduced effective coupling, $C_{a_1}(\gamma\gamma) \equiv \frac{C_{a_1}^{\mathrm{eff}}(\gamma\gamma)}{C_{h_{\mathrm{SM}}}^{\mathrm{eff}}(\gamma\gamma)}$, can yield an effective limit on the mass of the lighter chargino through[2]

$$C_{a_1}(\gamma\gamma) \simeq \lambda \times \frac{130\ \mathrm{GeV}}{m_{\chi_1^\pm}}, \tag{8}$$

for $m_{a_1} \simeq 125$ GeV. The bound obtained on the mass of $\chi_1^\pm$ is also an effective upper limit on the mass of the lightest neutralino, χ ($\equiv \chi_1^0$).

Having described the mechanism for enhancing the $\gamma\gamma$ decay rate of a_1, we now discuss the actual quantity used for comparison with the experimentally observed $\gamma\gamma$ rate. In terms of the reduced effective couplings, $C_{a_1}(\gamma\gamma)$ and $C_{a_1}(dd)$, of a_1 to $\gamma\gamma$ and $b\bar{b}$, respectively, the signal rate, given in Eq. (1), can be rewritten for the $b\bar{b}h$ production mode as

$$R_{\gamma\gamma}^{bb}(a_1) = C_{a_1}^2(dd)C_{a_1}^2(\gamma\gamma)\frac{\Gamma_{h_{\mathrm{SM}}}^{\mathrm{total}}}{\Gamma_{a_1}^{\mathrm{total}}} \simeq |P_{11}''|^2\lambda^2\left(\frac{130\ \mathrm{GeV}}{m_{\chi_1^\pm}}\right)^2\left(\frac{1}{\Gamma_{a_1}^{\mathrm{total}}/\Gamma_{h_{\mathrm{SM}}}^{\mathrm{total}}}\right), \tag{9}$$

where $|P_{11}''| \simeq |\frac{\lambda(A_\lambda^{\mathrm{SUSY}} - 2\kappa s)v}{\mu(A_\lambda^{\mathrm{SUSY}} + \kappa s)}|$ and $\Gamma_{a_1}^{\mathrm{total}}$ and $\Gamma_{h_{\mathrm{SM}}}^{\mathrm{total}}$ denote the theoretical values of the total widths of a_1 and a SM Higgs boson with the same mass as a_1, respectively. The dependence of the above expression on $\tan\beta$ is not straightforward, since it only enters indirectly through $\Gamma_{h_{\mathrm{SM}}}^{\mathrm{total}}/\Gamma_{a_1}^{\mathrm{total}}$. Equation (9) also shows that, as noted in the introduction, the conditions necessary to enhance $C_{a_1}(\gamma\gamma)$, i.e., large λ and small μ, also yield an enhanced $|C_{a_1}(dd)| \simeq |P_{11}''|$.

In Sec. III we will use Eqs. (8) and (9) to obtain an effective upper limit on $m_{\chi_1^\pm}$ and the mass of χ, m_χ, in our model under consideration.

[2]Assuming a singletlike a_1, which implies $P_{13} \simeq 1$, and a Higgsino-like $\chi_1^\pm$ so that $\sin\theta_{U,V} \simeq 1$.

C. $b\bar{b}/\tau^+\tau^-$ decay of the pseudoscalar

The signal rate in these decay modes can be written, following Eq. (9), as

$$R^{bb}_{b\bar{b}/\tau^+\tau^-}(a_1) \simeq \frac{|P''_{11}|^4}{\Gamma^{\rm total}_{a_1}/\Gamma^{\rm total}_{h_{\rm SM}}}. \quad (10)$$

It should be noted in the above expression that both the $b\bar{b}$ and $\tau^+\tau^-$ decay rates scale with the same reduced coupling $C_{a_1}(dd)$. Both these decay channels, therefore, show exactly the same behavior as far as their signal rates are concerned, despite the fact that $\mathrm{BR}(a_1 \to \tau^+\tau^-)$ is considerably smaller than $\mathrm{BR}(a_1 \to b\bar{b})$. From an experimental point of view, the $b\bar{b}$ decay mode will result in 4 b jets, which may be quite challenging to tag owing to the large hadronic background, although this mode has been visited in the past [3]. The $\tau^+\tau^-$ decay mode, on the other hand, is subject to a much smaller leptonic background and is in fact the preferred mode for analyzing possibly supersymmetric Higgs bosons.

III. CNMSSM-NUHM

In the fully constrained NMSSM, universality conditions are imposed on the dimensionful parameters at the GUT scale. This leads to a unified gaugino mass parameter, $m_{1/2}$, besides m_0 and A_0, with A_λ and A_κ also unified to the latter. Thus, given the correct value of the mass of the Z boson, m_Z, m_0, $m_{1/2}$, A_0 and λ, taken as an input parameter at $M_{\rm SUSY}$, constitute the only free parameters in the CNMSSM.

In the partially unconstrained version of the model, the CNMSSM-NUHM, the soft masses of the Higgs fields, m_{H_u}, m_{H_d} and m_S, as well as the soft trilinear coupling parameters A_λ and A_κ are taken as free parameters at the GUT scale, instead of assuming their unification with m_0 and A_0, respectively. Through the minimization conditions of the Higgs potential the three mass parameters m_{H_u}, m_{H_d} and m_S at the electroweak scale can be traded for the parameters κ, $\mu_{\rm eff}$ and $\tan\beta$. The model is thus defined in terms of the following eight continuous input parameters:

$$m_0,\, m_{1/2},\, A_0,\, \tan\beta,\, \lambda,\, \kappa,\, \mu_{\rm eff},\, A_\lambda = A_\kappa.$$

The unification of A_λ and A_κ at the GUT scale assumed above is in general not necessary in the CNMSSM-NUHM. In fact, one can argue that the restriction on A_0 for $\mu_{\rm eff} < 0$ and the resultant tension between m_{h_1} and m_{a_1} discussed in the previous section can be relaxed by not imposing such a condition. In that case, the effect of large A_λ can be counterbalanced by increasing A_κ independently, thus still yielding physical a_1 solutions. However, this unification condition has a minimal impact on the allowed parameter space of the model for our purpose since, as we shall see later, we can still exploit the interesting phenomenology of the model while keeping the number of free parameters to a minimum. This is also consistent with the fully constrained version of the model that we studied earlier [14], where A_κ and A_λ were set equal to A_0 at the GUT scale, even though $m_S \neq m_0$.

IV. METHODOLOGY AND RESULTS

We perform scans of the parameter space of CNMSSM-NUHM, requiring both h_1 and a_1 to have masses near 125 GeV. We impose the latest 95% confidence level (C.L.) exclusion limit on the $(m_0, m_{1/2})$ space of mSUGRA/CMSSM obtained by the ATLAS Collaboration from two same-sign leptons and jets in the final state at $\sqrt{s} =$ 8 TeV with 20.7/fb of data [39]. It has been verified in Refs. [8,14] that such a limit, obtained originally for the CMSSM, generally has negligible dependence on the Higgs sector parameters and is, therefore, applicable to any R-parity conserving SUSY model with unified m_0 and $m_{1/2}$. We also impose the lower limit, $m_{\chi_1^\pm} >$ 94 GeV [33], on the lightest chargino mass in our scans. Furthermore, we include Gaussian likelihoods for the most significant b-physics observables, with their measured mean values and errors taken as:

(i) $\mathrm{BR}(\mathrm{B_s} \to \mu^+\mu^-) = (3.2^{+1.5}_{-1.2} \pm 0.32) \times 10^{-9}$,
(ii) $\mathrm{BR}(\mathrm{B_u} \to \tau\nu) = (1.66 \pm 0.66 \pm 0.38) \times 10^{-4}$, ,
(iii) $\mathrm{BR}(\bar{\mathrm{B}} \to X_s\gamma) = (3.43 \pm 0.22 \pm 0.21) \times 10^{-4}$ and
(iv) $\Delta M_{B_s} = (17.72 \pm 0.04 \pm 2.4)\ \mathrm{ps}^{-1}$.

For testing the compatibility of the regions of interest against the dark matter direct detection cross section, $\sigma_p^{\rm SI}$, we use the XENON100 90% C.L. exclusion limits [40]. Note that we neglect the a_μ constraint here since it is well known that the regions where correct a_μ can be obtained in the parameter spaces of SUSY models with unification of squark and slepton soft masses are strongly disfavored by the direct SUSY searches at the LHC [8,14,41]. However, in order to minimize the deviation from experimental value of a_μ and also to release the tension between m_{h_1} and m_{a_1}, as discussed at the end of Sec. II A, we shall use $\mu_{\rm eff} > 0$, unless stated otherwise. We also note here that no likelihood function was implemented in our scans for the relic density constraint. However, in all our results below, we only show points with neutralino relic density, $\Omega_\chi h^2$, lying in the $\pm 2\sigma$ range, $0.087 < \Omega_\chi h^2 < 0.137$, around the central experimental value (again, unless stated otherwise), after taking into account 10% error on the theoretical calculation. We use a slightly extended range of the allowed Higgs boson mass, 122 GeV $< m_{h_1,a_1} <$ 130 GeV, compared to the mass measurements of the observed boson at the LHC in order to take into account large theoretical and experimental errors. Finally, for all the points considered, h_1 is always SM-like, with $R^{bb}_{X/V}(h_1) \simeq 1$.

The numerical analysis was performed using the BayesFITS package, which engages several external, publicly available tools: MultiNest [42] for sampling of the CNMSSM-NUHM parameter space; NMSSMTools v3.2.4 [43] for computing SUSY mass spectrum, Higgs branching ratios (BRs) and reduced couplings, as well as ΔM_{B_s} for a

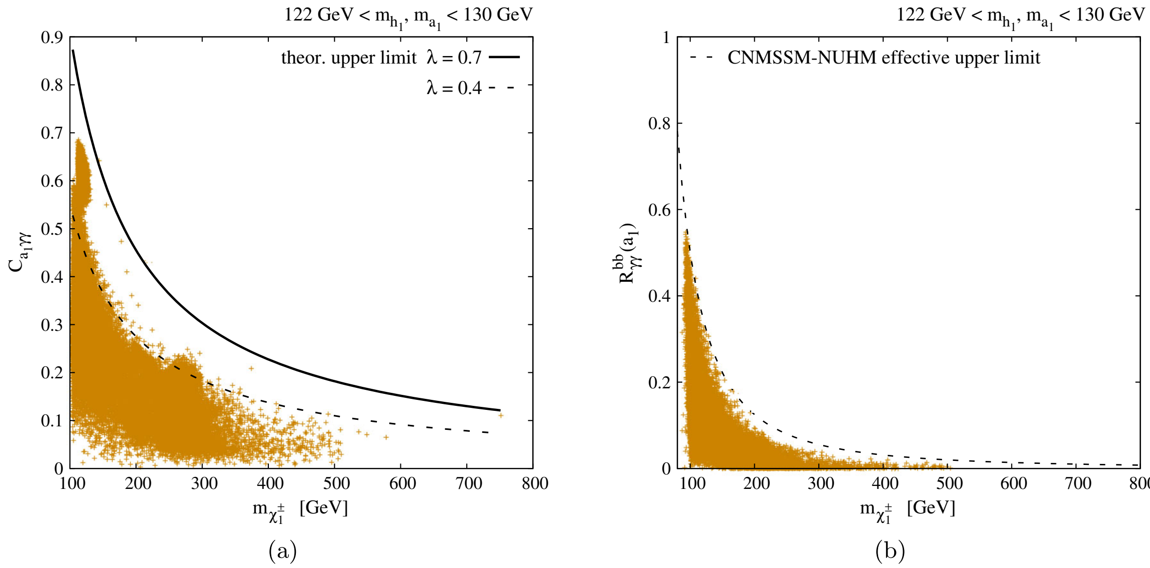

FIG. 1 (color online). (a) Distribution of points obtained in our scan of the CNMSSM-NUHM parameter space in the $(m_{\chi_1^\pm}, C_{a_1}(\gamma\gamma))$ plane. The dashed line shows the effective upper limit observed in the scan. The solid line is based on a perturbative upper limit on λ and is shown for comparison. (b) Distribution of points in the $(m_{\chi_1^\pm}, R^{bb}_{\gamma\gamma}(a_1))$ plane. The dashed line shows the effective upper limit observed in our scan.

given NMSSM point; and SuperIso v3.3 [44] for calculating $\mathrm{BR}(\bar{\mathrm{B}} \to \mathrm{X_s}\gamma)$, $\mathrm{BR}(\mathrm{B_s} \to \mu^+\mu^-)$ and $\mathrm{BR}(\mathrm{B_u} \to \tau\nu)$. DM observables such as the relic density and σ_p^{SI} are calculated with MicrOMEGAs v2.4.5 [45].

A. $\gamma\gamma$ rate enhancement

As noted in Sec. II, the scenario under consideration requires low values of μ_{eff} giving a light Higgsino-like $\chi_1^\pm$ and correspondingly a χ with significant Higgsino component. Under these conditions the upper limit on $m_{\chi_1^\pm}$ and m_χ can be obtained in the CNMSSM-NUHM from Fig. 1, where $C_{a_1}(\gamma\gamma)$ and $R^{bb}_{\gamma\gamma}(a_1)$ are shown as functions of $m_{\chi_1^\pm}$ in a and b, respectively. For all points in the plots, we assume 122 GeV $< m_{h_1,a_1} <$ 130 GeV.

The parameter space of the CNMSSM-NUHM giving an enhancement in the $\gamma\gamma$ rate due to a ~125 GeV a_1 can in fact be divided into three main regions depending on the composition of χ:

(i) the singlino-Higgsino region,
(ii) the Higgsino region, and
(iii) the focus-point (FP) region.

Below we discuss the results for each of these regions separately.

1. Singlino-Higgsino region

This region is defined by χ being a mixture of a large Higgsino component and a smaller but important singlino component. Owing to the significant singlino component (20%–30%), the neutralino will interact very weakly with matter and will thus result in large relic abundance unless it has a small mass and consequently large annihilation cross section. In Fig. 2(a) we see the distribution of this region in the $(m_0, m_{1/2})$ plane. Light blue squares correspond to points with $1 < R^{bb}_{\gamma\gamma}(h_1 + a_1) \le 1.15$, green squares to points with $1.15 < R^{bb}_{\gamma\gamma}(h_1 + a_1) \le 1.3$, red squares to points with $1.3 < R^{bb}_{\gamma\gamma}(h_1 + a_1) \le 1.45$ and blue squares to points with $R^{bb}_{\gamma\gamma}(h_1 + a_1) > 1.45$. Also shown in the figure is the current 95% C.L. exclusion limit from ATLAS obtained with 20/fb of data.

While m_0 is widely distributed, intermediate-to-large values of $m_{1/2}$ are favored for allowing a neutralino with a negligible bino component for small positive μ_{eff}. In Fig. 2(b) the favored ranges of $\tan\beta$ and A_0 parameters are shown. We see that the enhancement in $R^{bb}_{\gamma\gamma}(h_1 + a_1)$ decreases as $\tan\beta$ increases. The reason for this is as follows. The enhancement in $R^{bb}_{\gamma\gamma}(a_1)$ grows with λ, according to Eq. (9). However, large values of λ can only give correct m_{h_1} for not too large values of $\tan\beta$. This is because larger values of $\tan\beta$ result in an enhanced Yukawa coupling of h_1 to $b\bar{b}$ and $\tau\bar{\tau}$. This will make A_λ run upward faster from its GUT scale value, which in turn causes A_κ to run downward to larger negative values. That will result in a decrease in m_{h_1}, since it has a significant singlet component, while m_{a_1} increases. A_0 almost always takes large negative values, in order to maximize m_{h_1}. We, therefore, hardly see any points corresponding to positive A_0.

In Fig. 2(c) we show the distribution of points in the (A_0, A_κ) plane. The interdependence of A_0 and $A_\lambda = A_\kappa$ is further illustrated by this figure. A_κ can take quite large positive values at the GUT scale, even though it ought to be negative at M_{SUSY}. The reason is that, for large negative A_0 values, A_λ, which is also positive, makes A_κ

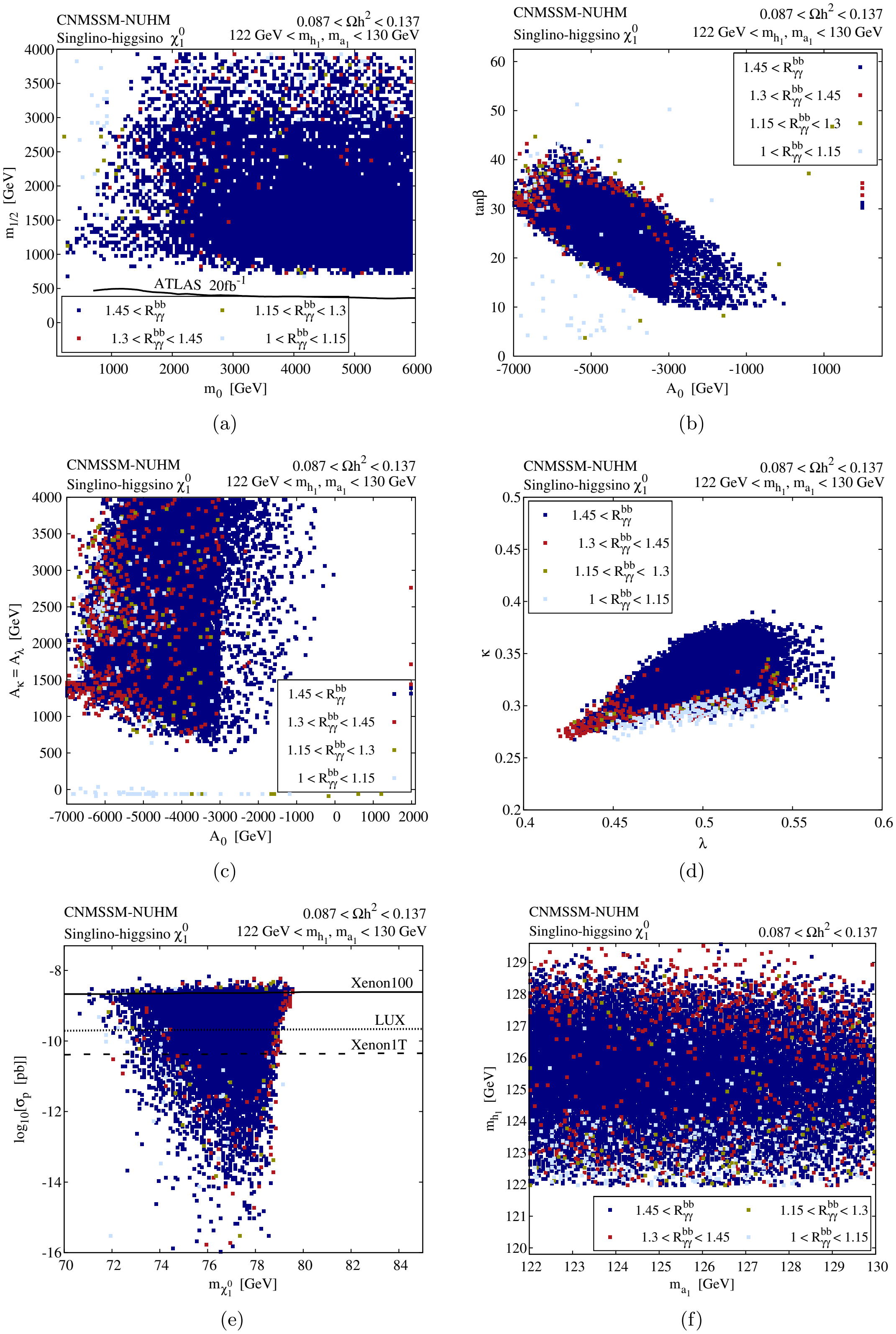

FIG. 2 (color online). (a)–(d) Ranges of CNMSSM-NUHM paramaters corresponding to the singlino-higgsino region. (e) σ_p^{SI} obtained for this region as a function of m_χ. (f) Ranges of m_{h_1} and m_{a_1} obtained in this region. See text for details.

run downward. In Fig. 2(d) the (λ, κ) plane is shown. The allowed range of λ for a given region is subject to a three-way tension. Large λ is favored in order to obtain an enhancement in the coupling of a_1 to $\chi_1^{\pm}$, but the condition to obtain a SM-like h_1, on the other hand, prefers smaller values. The small-to-intermediate range of λ seen in the figure is then a result of the compromise between these two conditions and, additionally, of the requirement to achieve the desired m_{a_1} by generating s $(= \mu_{\mathrm{eff}}/\lambda)$ of the correct size. We note also in the figure small-to-intermediate values of κ, which are required to maximize the singlino component of χ, as the 5×5 term in the neutralino mass matrix is equal to $2\kappa s$ $(\equiv 2\kappa\mu_{\mathrm{eff}}/\lambda)$. Hence, the smallness in κ has to be compensated by large values of A_κ, as noted in Fig. 2(c), for obtaining the correct m_{a_1}. Finally, over the entire allowed ranges of λ and κ, a large enhancement in $R_{\gamma\gamma}^{bb}(h_1 + a_1)$ is observed, although this region corresponds to more fine-tuned values of these two parameters compared to the other two regions, as we shall see later.

In Fig. 2(e) we show the $(m_\chi, \sigma_p^{\mathrm{SI}})$ plane for this region. Also shown in the figure are the actual 90% C.L. exclusion limits from XENON100 as well as the 90% C.L. limits expected from the LUX [46] and XENON1T [47] experiments. A large number of points satisfying the XENON100 limit lies below the projected 90% C.L. XENON1T limit. Note also that since very small m_χ and consequently $m_{\chi_1^\pm}$ is favored by this region almost all the points below the XENON100 line have a highly enhanced $R_{\gamma\gamma}^{bb}(a_1)$, since $\chi_1^\pm$ also appears in the denominator of Eq. (9). This is also the reason why such points are achievable even with relatively small values of $\tan\beta$, as seen in Fig. 2(b) earlier. This region yields the maximum enhancement, up to $\sim$60% or so, in $R_{\gamma\gamma}^{bb}(h_1 + a_1)$ out of the three regions discussed here and is, therefore, the most favorable of all.

In Fig. 2(f) we show the distribution of m_{h_1} vs that of m_{a_1}. We note that this region can have fairly large m_{h_1}, which is due to the combined effects of large negative A_0 as well as larger allowed values of λ. Another important feature of this region is that h_2 can also be almost mass degenerate with h_1 and a_1, implying in that case a "triple degeneracy" among the Higgses. Again, while mass degenerate h_1 and h_2 can explain the enhanced $\gamma\gamma$ rate in the ggh production mode in the ATLAS data, in order to test the additional degeneracy with a_1, one will have to explore the associated production mode of Higgs with $b\bar{b}$. In the $b\bar{b}h$ production mode, such h_2 can further contribute $\sim$20% of the measured $\gamma\gamma$ rate. Finally, $\mathrm{BR}(\mathrm{B_s} \to \mu^+\mu^-)$ in this region varies between 3×10^{-9} and 3.8×10^{-9}, while $\mathrm{BR}(\bar{\mathrm{B}} \to \mathrm{X_s}\gamma)$ lies in the 2.8×10^{-4} to 3.3×10^{-4} range.

2. Higgsino region

A nearly pure Higgsino-like neutralino can generate large enough $\Omega_\chi h^2$ only if $m_\chi \simeq \mu_{\mathrm{eff}} \sim 1$ TeV, but such high values of μ_{eff} will not yield the desired enhancement in the $a_1 \to \gamma\gamma$ rate. Therefore, in order to obtain a sizeable enhancement, one has to relax the condition on neutralino relic density (thereby allowing low μ_{eff} and, therefore, $\Omega_\chi h^2$ to be too low). One can assume that a neutralino contributes only partially to the relic abundance of the universe beside some other DM candidate, e.g., the axion. In that case $\Omega_\chi h^2 = \xi \Omega_{\mathrm{total}} h^2$, where ξ is the fraction of the total relic abundance produced by χ and $\Omega_{\mathrm{total}} h^2 = 0.112$. Another possibility is that the entire relic abundance is due to an alternative DM candidate particle in the model. Often considered examples of such an additional/alternative DM candidate are the gravitino (see, e.g., Ref. [48] for recent analyses in the MSSM) and/or axino [49]. The first (second) of these candidates is (not) tightly constrained by big bang nucleosynthesis, but both are likely to be allowed in this region due to the low neutralino yield at freeze-out.

In Fig. 3(a) we show the region in the $(m_0, m_{1/2})$ plane generating a light a_1 and a Higgsino-like χ. The color assignment of the points is the same as in the singlino-Higgsino region. Large values of m_0 are preferred again in order to enhance m_{h_1} through radiative corrections from the SUSY sector. $m_{1/2}$ also takes large values in order to minimize the bino component of χ with large μ_{eff}–$m_{1/2}$ splitting. In Fig. 3(b) we see that once again $\tan\beta$ spans a fairly wide range but small to intermediate values are favored by $R_{\gamma\gamma}^{bb}(\mathrm{a}_1)$, for the same reasons as in the singlino-Higgsino region. Larger values of negative A_0 are favored so that m_{h_1} can be maximized.

In Fig. 3(c) we show A_κ vs A_0. As in the singlino-Higgsino region, for the (comparatively smaller) positive A_κ at the GUT scale, only large negative A_0 values are allowed. However, in contrast with that region, a considerable number of points is visible for negative A_κ and negative A_0 up to ~ -2 TeV. In this portion of the region, negative A_0 makes A_λ run upward between the GUT scale and M_{SUSY} and, since the latter is negative, it also drives A_κ upward to smaller negative values. Naturally then, negative A_0 should not be very large, or A_κ at M_{SUSY} will be driven positive. Positive A_0 solutions are also possible as long as they do not yield positive A_κ at M_{SUSY}. In Fig. 3(d) the ranges of the paramaters λ and κ favored by our scenario under consideration are shown for this region. A larger range of κ is favored in this region compared to the singlino-Higgsino region since s is more free to vary owing to the comparatively less constrained A_κ (which does not need to be as large to give correct m_{a_1}). λ can now take much smaller values than those allowed in the singlino-Higgsino region but cannot be as large as there. This is in fact the main feature distinguishing this region from the singlino-Higgsino region in terms of the parameter space of the model. Evidently, larger enhancement in the $\gamma\gamma$ rate is favored by large values of λ.

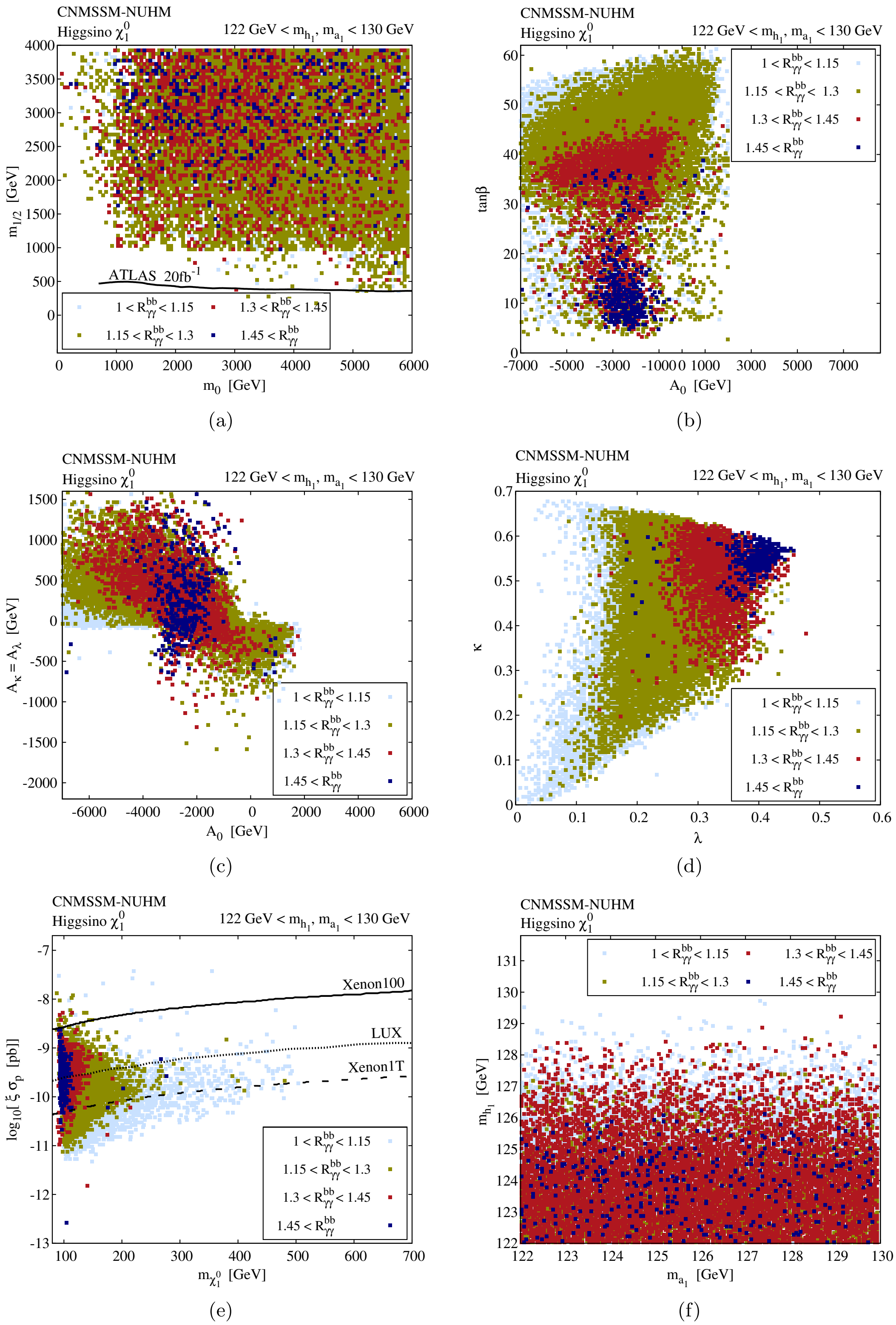

FIG. 3 (color online). (a)–(d) Ranges of CNMSSM-NUHM paramaters corresponding to the Higgsino region. (e) $\xi\sigma_p^{\rm SI}$ obtained for this region as a function of m_χ, where $\xi = \Omega_\chi h^2/\Omega_{\rm total}h^2$. (f) Ranges of m_{h_1} and m_{a_1} obtained in this region. See text for details.

In Fig. 3(e) we show the distribution of the points in the $(m_\chi, \xi\sigma_p^{\mathrm{SI}})$ plane for this region.[3] Almost all the points obtained in this region lie below the XENON100 line, and a portion of these points even lies below the projected XENON1T line. Since χ is almost purely Higgsino here, the smaller its mass, the bigger the enhancement in $R_{\gamma\gamma}^{bb}(a_1)$ is generated. Moreover, this region corresponds to large values of m_0 and $m_{1/2}$, so that the squarks and gluinos are always much heavier than the current LHC reach. Nevertheless, as discussed earlier, a more precise measurement of $R_{\gamma\gamma}^{bb}$ could still introduce limits on m_χ and $m_{\chi_1^\pm}$. Such derived upper limits are, therefore, especially interesting from the experimental point of view.

Finally, again as a result of large allowed values of negative A_0, h_1 as heavy as 129 GeV can be obtained in this region, as can be seen in Fig. 3(f). a_1 mass is evenly distributed in the defined range, almost always showing a large enhancement in the $\gamma\gamma$ rate. Finally a majority of points in this region shows a big enhancement, up to $\sim$50% above the SM expectation, in the $\gamma\gamma$ rate. We also note here that both $\mathrm{BR}(\mathrm{B_s} \to \mu^+\mu^-)$ and $\mathrm{BR}(\bar{\mathrm{B}} \to \mathrm{X_s}\gamma)$ always lie around their respective SM values.

3. Focus-point region

A light neutralino with mixed bino-Higgsino composition can generate correct DM relic density, $\Omega_\chi h^2$, in the so-called FP region of minimal SUSY models in general [50]. Since this region satisfies the constraints from XENON100 and $\mathrm{BR}(\bar{\mathrm{B}} \to \mathrm{X_s}\gamma)$ measurement better when $\mu_{\mathrm{eff}} < 0$ [51], we shall pursue this case here. In Fig. 4(a) we show the region in the $(m_0, m_{1/2})$ plane generating a light a_1 (122 GeV $\leq m_{a_1} \leq$ 130 GeV) and χ with a dominant bino and a small Higgsino component. We see that while large values of m_0 are favored in order to enhance the mass of h_1, $m_{1/2}$ is typically low, which is necessary for producing a mixed bino-Higgsino χ. This region, however, lies very close to the current 95% C.L. exclusion limit from ATLAS and should potentially be tested soon.

In Fig. 4(b) we show the favored ranges of the A_0 and $\tan\beta$ parameters. $\tan\beta$ is almost always $\gtrsim 5$ to allow enhancement in the $h_1 b\bar{b}$ coupling in our considered Higgs production mode, as noted earlier. However, we see in the figure that for high positive A_0, $\tan\beta$ is limited to small values, $\lesssim 15$. The reason is that large $\tan\beta$ results in an enhanced Yukawa coupling of h_1 to $b\bar{b}$ and $\tau\bar{\tau}$. Consequently A_λ runs downward rapidly from its GUT scale value (we shall see below that large positive A_0 coincides with negative A_λ) to more negative values at M_{SUSY}. This in turn causes A_κ to run upward from its GUT scale value, raising m_{a_1} beyond the desired range. The effective upper bound on $\tan\beta$ is relaxed for lower $|A_0|$, when the running is slower. We point out here that the opposite effect of $\tan\beta$ was noted in the other two regions due to the fact that there A_0 was negative, which made A_λ and A_κ run in the opposite directions to those here.

In Fig. 4(c) we show the distribution of the parameters A_0 and $A_\kappa = A_\lambda$ at the GUT scale. We notice that A_0 stops at much smaller negative values than it would be expected to take in order to maximize m_{h_1}. This is due to the reason explained in Sec. II. The main contribution to m_{a_1} comes from the leading term in Eq. (3). Since in this region we assume $\mu_{\mathrm{eff}} < 0$, A_0 is strongly bounded from below in order to minimize the effect of the second term there. Such negative A_0, by causing positive A_λ to run upward, also pushes A_κ to somewhat large positive values at the GUT scale, resulting in its small positive values at M_{SUSY}, since it runs in the opposite direction to A_λ. This is also the reason why no points are visible in the region with negative A_κ and negative A_0 as opposed to the Higgsino region, but conversely one can see some points with positive A_κ and positive A_0. Finally, for negative A_κ large positive A_0 can be reached, since such values of A_0 drive positive A_λ at the GUT scale downward, which in turn causes A_κ to run upward to positive values at M_{SUSY}.

Figure 4(d) shows the ranges of λ and κ corresponding this scenario. The distribution of these two parameters almost mimics that in the Higgsino region, and as in there larger values of enhancement in $R_{\gamma\gamma}^{bb}(h_1 + a_1)$ are obtained for large λ. In Fig. 4(e) we show how the FP region fares against the XENON100 limits. Note that m_χ is bounded from below by the ATLAS limit on $m_{1/2}$ in this region as it is bino-dominated. We see that a majority of the allowed points with an enhanced $\gamma\gamma$ rate lie below the XENON100 line. Most of this region, however, lies above the LUX limit, while the XENON1T data should be able to test almost all of it. Figure 4(f) shows the allowed masses of h_1 and a_1 in this region. We see that m_{h_1} is always lighter than 124 GeV, which is a consequence of $\mu_{\mathrm{eff}} < 0$ not allowing very large values of negative A_0 in this region, as discussed above. a_1, on the other hand, can easily have a mass greater than 125 GeV.

Overall, we notice only a relatively small enhancement, up to $\sim$25%, in the $\gamma\gamma$ rate compared to the SM expectation in this region of the CNMSSM-NUHM parameter space. The reason for this is that $m_{\chi_1^\pm}$ is not allowed to take values even as small as those possible in the Higgsino region due to the lower bound on the mass of χ discussed above ($m_{\chi_1^\pm} \simeq \mu_{\mathrm{eff}} > m_\chi$). $\mathrm{BR}(\mathrm{B_s} \to \mu^+\mu^-)$ in this region varies between 2×10^{-9} and 5.5×10^{-9}, which is within 2σ of the experimentally measured value 3.2×10^{-9}, taking into account the theoretical error (as in Ref. [14]). On the other hand, $\mathrm{BR}(\bar{\mathrm{B}} \to \mathrm{X_s}\gamma)$ takes values between 3.1×10^{-4} and 3.7×10^{-4} and hence is always close to the experimental value. This region, owing mainly to the facts that m_{h_1} finds it difficult to reach the experimentally observed value and that the reduced $\gamma\gamma$ rate of a_1 barely

[3]The figure assumes that χ is only responsible for a small portion of the observed relic abundance. For the points obtained in the scan, $\xi \leq 0.05$.

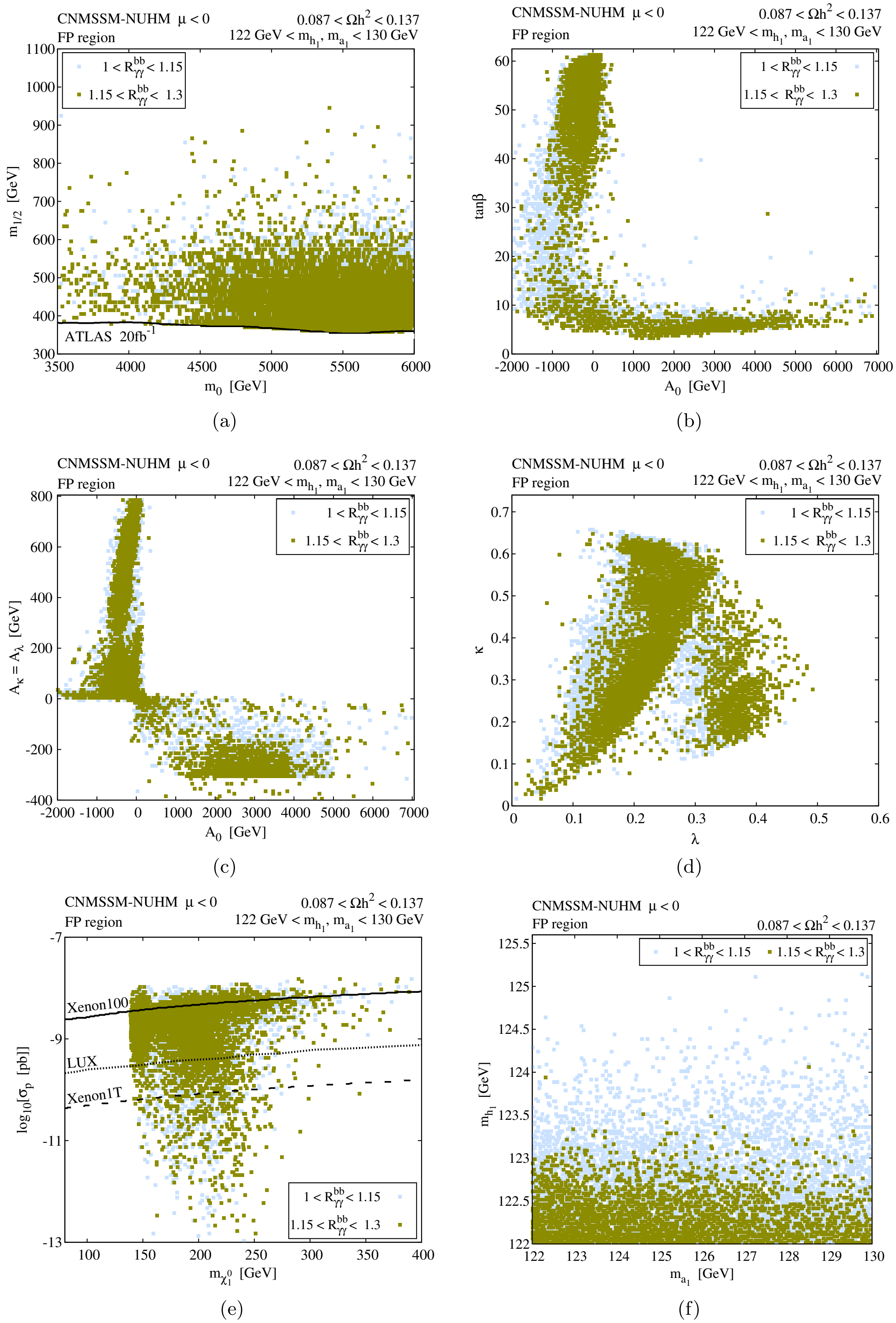

FIG. 4 (color online). (a)–(d) Ranges of CNMSSM-NUHM paramaters corresponding to the FP region. (e) $\sigma_p^{\rm SI}$ obtained for this region as a function of m_χ. (f) Ranges of m_{h_1} and m_{a_1} obtained in this region. See text for details.

exceeds 0.25, is the least favored of the three regions explored here.

To summarize, in Fig. 5(a) we show the range of m_χ across all the regions for which an enhancement in $R^{bb}_{\gamma\gamma}(h_1 + a_1)$ was obtained in our CNMSSM-NUHM scan and its compatibility with the current and expected limits on $\sigma_p^{\rm SI}$. These regions are identified separately in Fig. 5(b), again, in the $(m_\chi, \xi\sigma_p^{\rm SI})$ plane, where the orange squares denote the FP region, dark green squares the Higgsino region and brown squares the singlino-Higgsino region.

B. $b\bar{b}/\tau^+\tau^-$ rate enhancement

In this subsection we highlight only the important features corresponding to the $b\bar{b}$ and $\tau^+\tau^-$ decay channels of a_1 for the three regions discussed in detail above. As noted in Sec. II C, contrary to the case of a MSSM-like scalar Higgs boson, $\tan\beta$ affects the $b\bar{b}/\tau^+\tau^-$ rate of a_1 only

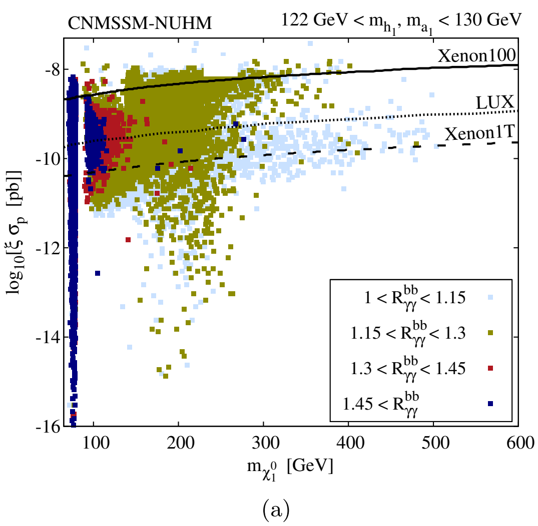

FIG. 5 (color online). (a) The range of $\sigma_p^{\rm SI}$ for giving an enhancement in $R^{bb}_{\gamma\gamma}(h_1 + a_1)$ vs the neutralino mass m_χ. Also shown are the 90% C.L. exclusion limits from XENON100 as well as the 90% C.L. limits expected from the LUX and XENON1T experiments. $\xi = \Omega_\chi h^2/\Omega_{\rm total} h^2$ when χ is almost purely Higgsino but 1 otherwise. (b) The $(m_\chi, \sigma_p^{\rm SI})$ plane showing the three CNMSSM-NUHM regions where $R^{bb}_{\gamma\gamma}(h_1 + a_1)$ is enhanced. Maroon squares denote the singlino-Higgsino region, green squares the Higgsino region and yellow squares the FP region. $\xi = \Omega_\chi h^2/\Omega_{\rm total} h^2$ in the Higgsino region but 1 in the singlino-Higgsino and FP regions.

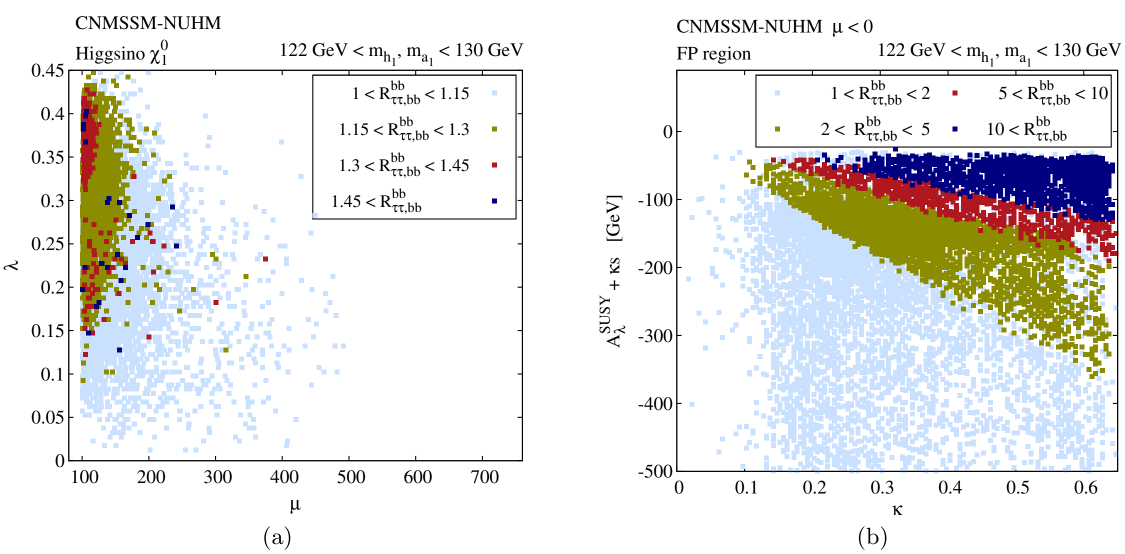

FIG. 6 (color online). (a) Enhancement in $R^{bb}_{b\bar{b}/\tau^+\tau^-}(h_1 + a_1)$ obtained in the Higgsino region as a function of the λ and $\mu_{\rm eff}$ parameters. (b) Enhancement in $R^{bb}_{b\bar{b}/\tau^+\tau^-}(h_1 + a_1)$ obtained in the FP region as a function of κ and $(A_\lambda^{\rm SUSY} + \kappa s)$ from the denominator of $|P''_{11}|$. See the text for details.

indirectly through the term in the denominator of Eq. (10). Instead, a sizable $R^{bb}_{b\bar{b}/\tau^+\tau^-}(a_1)$ is an additional consequence of the conditions necessary to obtain an enhancement in $R^{bb}_{\gamma\gamma}(a_1)$, i.e., large λ and small $\mu_{\rm eff}$. This is demonstrated in Fig. 6(a) for the Higgsino region, where one can see that the enhancement in $R^{bb}_{b\bar{b}/\tau^+\tau^-}(h_1 + a_1)$ rises with increasing λ and decreasing $\mu_{\rm eff}$. In the singlino-Higgsino region (not shown in the figure), $R^{bb}_{b\bar{b}/\tau^+\tau^-}(h_1 + a_1)$ is always larger than 1.6 for the entire range of λ, seen in Fig. 2(d) and can be as high as 1.9. It will therefore result in a small blue region at the top left corner of Fig. 6(a).

In the FP region, $R^{bb}_{b\bar{b}/\tau^+\tau^-}(a_1)$ can in fact have extremely large values, $\sim$100. However, this should not be interpreted as a characteristic feature specific to the FP region but as a result of negative $\mu_{\rm eff}$ assumed for this region. $R^{bb}_{b\bar{b}/\tau^+\tau^-}(a_1)$ increases as the denominator, $A^{\rm SUSY}_\lambda + \kappa s$, of $|P''_{11}|$ in Eq. (10) approaches zero. For small negative $\mu_{\rm eff}$ and large positive λ, resulting in small negative s, the size of the denominator reduces as κ grows. In Fig. 6(b) we show how $R^{bb}_{b\bar{b}/\tau^+\tau^-}(h_1 + a_1)$ enhances with increasing κ and the decreasing value of the above denominator term and can acquire a huge value before the perturbative upper limit on the former is reached. Evidently a similar effect of negative $\mu_{\rm eff}$ should manifest in the other two regions also. However, since negative $\mu_{\rm eff}$ causes a tension between m_{a_1} and m_{h_1} and does not allow both of these to be around 125 GeV, as discussed in detail in Sec. II A and as noted in the FP region, we retain $\mu_{\rm eff} > 0$ in the singlino-Higgsino and the Higgsino regions. We thus expect the enhancement in the $b\bar{b}/\tau^+\tau^-$ channels to be larger in these two regions also for $\mu_{\rm eff} < 0$, but at the cost of m_{h_1} and a_μ lying far from their respective experimentally measured values.

V. SUMMARY

We have proposed an experimental test of a scenario in the NMSSM in which the lightest pseudoscalar of the model as well a SM-like lightest scalar boson both have masses around $\sim$125 GeV. The pseudoscalar could be distinguishable from the scalar at the LHC in the associated Higgs production mode with a $b\bar{b}$ pair in the final state. This is because it will contribute significantly to the observed signal rate in the $\gamma\gamma$ and $b\bar{b}/\tau^+\tau^-$ channels, but, since a pseudoscalar does not couple to W and Z bosons, the measured rate in the WW/ZZ channels will be due only to the scalar and therefore SM-like. We have discussed the conditions necessary to obtain a_1 with the correct mass and noted that an observable enhancement in its $\gamma\gamma$ decay rate is made possible by a light chargino entering in its one-loop effective coupling to two photons. We have also discussed in detail how the conditions to obtain such a light chargino in turn lead to an enhancement in the $b\bar{b}$ and $\tau^+\tau^-$ rates also. We have argued that, due to very specific requirements on the composition of a_1, which should be singletlike, and of the light chargino, which should be almost purely Higgsino-like, such a scenario cannot be realized in the MSSM and is extremely unlikely in the fully constrained NMSSM.

We have, therefore, analyzed the CNMSSM with the universality conditions lifted in the Higgs sector to study the scenario at hand. We have scanned the parameter space of this model in order to look for regions that can allow both $\chi_1^\pm$ and a_1 with the desired masses and compositions. We have found that these regions can be divided into three broad types based on the composition of the neutralino which, owing to the condition on $\chi_1^\pm$, should also have a large Higgsino component. These regions include the singlino-Higgsino region, where χ is Higgsino-dominated but with an admixture of the singlino; the Higgsino region, where it is almost purely Higgsino; and the FP region, where it is a bino-Higgsino mixture. The region showing the least enhancement in the $\gamma\gamma$ rate of a_1 is the FP region, where it only reaches up to $\sim$25%, while the most favored one is the mixed Higgsino-singlino region, where the enhancement can be as high as $\sim$60%. However, we noted that for negative $\mu_{\rm eff}$, the FP region satisfies the constraints from $\sigma_p^{\rm SI}$ and ${\rm BR}(\bar{\rm B} \to {\rm X_s}\gamma)$ better and can also have a very large enhancement in the $b\bar{b}$ and $\tau^+\tau^-$ rates but cannot yield m_{h_1} greater than 124 GeV.

We have also stressed the fact that such a singletlike a_1 is likely to remain invisible at the LHC in the gluon-fusion production channel. The reason is that while the effective coupling of a_1 to the $\gamma\gamma$, $b\bar{b}$ and $\tau^+\tau^-$ pairs gets enhanced, the effective coupling to two gluons is still highly suppressed compared to a SM-like Higgs boson. We have, therefore, emphasized that a more focused analysis of the associated Higgs boson production mode with $b\bar{b}$ pair, which is the least favorable production mode for a SM-like Higgs boson, is essential. By revealing such a pseudoscalar through the triple enhancement in its decay rates, this production mode could provide a clear signature of our considered NMSSM scenario, in particular, and of beyond the SM physics, in general.

ACKNOWLEDGMENTS

The authors would like to thank Y.-L. Sming Tsai for valuable discussions and inputs. They are also thankful to A. Kalinowski and M. Pierini for their important remarks about the $b\bar{b}h$ production mode. This work has been funded in part by the Welcome Programme of the Foundation for Polish Science. L. R. is also supported in part by the Polish National Science Centre Grant No. N202 167440, an STFC consortium grant of Lancaster, Manchester and Sheffield Universities, and by the EC 6th Framework Programme MRTN-CT-2006-035505. The use of the CIS computer cluster at NCBJ is gratefully acknowledged.

[1] S. Chatrchyan *et al.* (CMS Collaboration), Phys. Lett. B **716**, 30 (2012).
[2] G. Aad *et al.* (ATLAS Collaboration), Phys. Lett. B **716**, 1 (2012).
[3] twiki.cern.ch/twiki/bin/view/CMSPublic/PhysicsResultsHIG.
[4] twiki.cern.ch/twiki/bin/view/AtlasPublic/HiggsPublicResults.
[5] G. Aad *et al.* (ATLAS Collaboration), Report No. ATLAS-CONF-2013-034, 2013.
[6] D. J. Chung, A. J. Long, and L.-T. Wang, Phys. Rev. D **87**, 023509 (2013); H. Baer *et al.*, arXiv:1210.3019; Z. Heng, arXiv:1210.3751; M. Carena, S. Gori, I. Low, N. Shah, and C. Wagner, J. High Energy Phys. 02 (2013) 114; P. Bechtle, S. Heinemeyer, O. Stål, T. Stefaniak, G. Weiglein, and L. Zeune, Eur. Phys. J. C **73**, 2354 (2013); D. Berenstein, T. Liu, and E. Perkins, Phys. Rev. D **87**, 115004 (2013); K. Cheung, C.-T. Lu, and T.-C. Yuan, Phys. Rev. D **87**, 075001 (2013); J. Cao, L. Wu, P. Wu, and J. M. Yang, arXiv:1301.4641.
[7] A. Fowlie, M. Kazana, K. Kowalska, S. Munir, L. Roszkowski, E. Maria Sessolo, S. Trojanowski, and Y.-L. Sming Tsai, Phys. Rev. D **86**, 075010 (2012).
[8] K. Kowalska, L. Roszkowski, and E. M. Sessolo, J. High Energy Phys. 06 (2013) 078.
[9] S. King, M. Muhlleitner, and R. Nevzorov, Nucl. Phys. **B860**, 207 (2012); J. Cao, Z. Heng, J. Min Yang, Y. Zhang, and J. Zhu, J. High Energy Phys. 03 (2012) 086; D. A. Vasquez, G. Bélanger, C. Bœhm, J. Da Silva, P. Richardson, and C. Wymant, Phys. Rev. D **86**, 035023 (2012); K. S. Jeong, Y. Shoji, and M. Yamaguchi, J. High Energy Phys. 09 (2012) 007; J. Rathsman and T. Rossler, Adv. High Energy Phys. **2012**, 1 (2012); D. Das, U. Ellwanger, and P. Mitropoulos, J. Cosmol. Astropart. Phys. 08 (2012) 003; J. Cao, Z. Heng, J. M. Yang, and J. Zhu, J. High Energy Phys. 10 (2012) 079.
[10] J. F. Gunion, Y. Jiang, and S. Kraml, Phys. Rev. D **86**, 071702 (2012).
[11] K. J. Bae, K. Choi, E. Jin Chun, S. Hui Im, C. Beom Park, and C. Sub Shin, J. High Energy Phys. 11 (2012) 118; T. Cheng *et al.*, arXiv:1207.6392; Z. Kang, T. Li, J. Li, and Y. Liu, arXiv:1208.2673; M. Perelstein and B. Shakya, arXiv:1208.0833; K. Schmidt-Hoberg and F. Staub, J. High Energy Phys. 10 (2012) 195; G. Belanger, U. Ellwanger, J. Gunion, Y. Jiang, and S. Kraml, arXiv:1208.4952.
[12] J. F. Gunion, Y. Jiang, and S. Kraml, Phys. Rev. Lett. **110**, 051801 (2013).
[13] K. Agashe, Y. Cui, and R. Franceschini, J. High Energy Phys. 02 (2013) 031; G. Chalons and F. Domingo, Phys. Rev. D **86**, 115024 (2012); I. Gogoladze, B. He, and Q. Shafi, Phys. Lett. B **718**, 1008 (2013); G. Belanger, U. Ellwanger, J. F. Gunion, Y. Jiang, S. Kraml, and J. H. Schwarz, J. High Energy Phys. 01 (2013) 069; H. Dreiner, F. Staub, and A. Vicente, Phys. Rev. D **87**, 035009 (2013); S. King, M. Mhlleitner, R. Nevzorov, and K. Walz, Nucl. Phys. **B870**, 323 (2013); K. Choi, S. H. Im, K. S. Jeong, and M. Yamaguchi, J. High Energy Phys. 02 (2013) 090; T. Gherghetta, B. von Harling, A. D. Medina, and M. A. Schmidt, J. High Energy Phys. 02 (2013) 032; D. E. Lopez-Fogliani, J. Phys. Conf. Ser. **384**, 012014 (2012); J. Cao, Z. Heng, L. Shang, P. Wan, and J. M. Yang, J. High Energy Phys. 04 (2013) 134; D. Das, U. Ellwanger, and A. M. Teixeira, J. High Energy Phys. 04 (2013) 117; D. G. Cerdeno, P. Ghosh, and C. B. Park, J. High Energy Phys. 06 (2013) 031; N. D. Christensen, T. Han, Z. Liu, and S. Su, J. High Energy Phys. 08 (2013) 019; W. Wang, J. M. Yang, and L. L. You, J. High Energy Phys. 07 (2013) 158; R. Barbieri, D. Buttazzo, K. Kannike, F. Sala, and A. Tesi, Phys. Rev. D **87**, 115018 (2013); S. Moretti, S. Munir, and P. Poulose, arXiv:1305.0166.
[14] K. Kowalska, S. Munir, L. Roszkowski, E. M. Sessolo, S. Trojanowski, and Y.-L. Sming Tsai, Phys. Rev. D **87**, 115010 (2013).
[15] P. Athron, S. King, D. Miller, S. Moretti, and R. Nevzorov, Phys. Rev. D **86**, 095003 (2012); L. Basso and F. Staub, Phys. Rev. D **87**, 015011 (2013); K. Schmidt-Hoberg, F. Staub, and M. W. Winkler, J. High Energy Phys. 01 (2013) 124; K. Benakli, M. D. Goodsell, and F. Staub, J. High Energy Phys. 06 (2013) 073.
[16] G. L. Kane, C. F. Kolda, L. Roszkowski, and J. D. Wells, Phys. Rev. D **49**, 6173 (1994).
[17] M. Drees, Int. J. Mod. Phys. A **04**, 3635 (1989).
[18] J. Ellis, J. F. Gunion, H. E. Haber, L. Roszkowski, and F. Zwirner, Phys. Rev. D **39**, 844 (1989).
[19] U. Ellwanger, C. Hugonie, and A. M. Teixeira, Phys. Rep. **496**, 1 (2010).
[20] M. Maniatis, Int. J. Mod. Phys. A **25**, 3505 (2010).
[21] U. Ellwanger, J. High Energy Phys. 03 (2012) 044.
[22] R. Benbrik, M. Gomez Bock, S. Heinemeyer, O. Stål, G. Weiglein, and L. Zeune, Eur. Phys. J. C **72**, 2171 (2012).
[23] A. Djouadi, U. Ellwanger, and A. Teixeira, Phys. Rev. Lett. **101**, 101802 (2008).
[24] A. Djouadi, U. Ellwanger, and A. Teixeira, J. High Energy Phys. 04 (2009) 031.
[25] J. F. Gunion, Y. Jiang, and S. Kraml, Phys. Lett. B **710**, 454 (2012).
[26] U. Ellwanger and C. Hugonie, Adv. High Energy Phys. **2012**, 1 (2012).
[27] S. Dawson, C. Jackson, L. Reina, and D. Wackeroth, Mod. Phys. Lett. A **21**, 89 (2006); S. Dawson, C. Jackson, and P. Jaiswal, arXiv:1110.2161.
[28] M. Badziak, M. Olechowski, and S. Pokorski, J. High Energy Phys. 06 (2013) 043.
[29] S. Chatrchyan *et al.* (CMS Collaboration), Phys. Rev. Lett. **110**, 081803 (2013).
[30] A. Djouadi and G. Moreau, arXiv:1303.6591.
[31] M. Spira, Fortschr. Phys. **46**, 203 (1998).
[32] A. Djouadi, Phys. Rep. **459**, 1 (2008).
[33] J. Beringer *et al.* (Particle Data Group Collaboration), Phys. Rev. D **86**, 010001 (2012).
[34] A. Djouadi, Phys. Rep. **457**, 1 (2008).
[35] N. D. Christensen, T. Han, and S. Su, Phys. Rev. D **85**, 115018 (2012).
[36] M. Carena, S. Heinemeyer, O. Stl, C. Wagner, and G. Weiglein, arXiv:1302.7033.
[37] S. Scopel, N. Fornengo, and A. Bottino, Phys. Rev. D **88**, 026506 (2013).
[38] C. Boehm, P. S. B. Dev, A. Mazumdar, and E. Pukartas, J. High Energy Phys. 06 (2013) 113.
[39] G. Aad *et al.* (ATLAS Collaboration), Report No. ATLAS-CONF-2013-007, 2013.
[40] E. Aprile *et al.* (XENON100 Collaboration), Phys. Rev. Lett. **109**, 181301 (2012).

[41] L. Roszkowski, E. M. Sessolo, and Y.-L. S. Tsai, Phys. Rev. D **86**, 095005 (2012).
[42] F. Feroz, M. Hobson, and M. Bridges, Mon. Not. R. Astron. Soc. **398**, 1601 (2009).
[43] www.th.u-psud.fr/NMHDECAY/nmssmtools.html.
[44] A. Arbey and F. Mahmoudi, Comput. Phys. Commun. **176**, 367 (2007).
[45] G. Belanger, F. Boudjema, A. Pukhov, and A. Semenov, Comput. Phys. Commun. **181**, 1277 (2010).
[46] D. Akerib *et al.* (LUX Collaboration), Nucl. Instrum. Methods Phys. Res., Sect. A **704**, 111 (2013).
[47] E. Aprile (XENON1T Collaboration), arXiv:1206.6288.
[48] S. Bailly, K.-Y. Choi, K. Jedamzik, and L. Roszkowski, J. High Energy Phys. 05 (2009) 103; L. Roszkowski, S. Trojanowski, K. Turzynski, and K. Jedamzik, J. High Energy Phys. 03 (2013) 013.
[49] L. Covi, J. E. Kim, and L. Roszkowski, Phys. Rev. Lett. **82**, 4180 (1999); L. Covi, H.-B. Kim, J. E. Kim, and L. Roszkowski, J. High Energy Phys. 05 (2001) 033; K.-Y. Choi, L. Roszkowski, and R. Ruiz de Austri, J. High Energy Phys. 04 (2008) 016.
[50] K. L. Chan, U. Chattopadhyay, and P. Nath, Phys. Rev. D **58**, 096004 (1998); J. L. Feng, K. T. Matchev, and T. Moroi, Phys. Rev. D **61**, 075005 (2000); J. L. Feng, K. T. Matchev, and F. Wilczek, Phys. Lett. B **482**, 388 (2000).
[51] L. Roszkowski, R. Ruiz de Austri, and R. Trotta, J. High Energy Phys. 07 (2007) 075.